MODELLING THE CORROSION AT LAP SPLICE JOINTS IN CONCRETE BEAMS

Amged O. Abdelatif [1], Joško Ožbolt [2], and Serena Gambarelli [3]

[1]Department of Civil Engineering Engineering, Faculty of Engineering, University of Khartoum, Amged.Abdelatif@uofk.edu

[2] Institute of Construction Materials, University of Stuttgart, Germany, 70569 Stuttgart, bozbolt@iwb.uni-stuttgart.de

[3] Institute of Construction Materials, University of Stuttgart, Germany, 70569 Stuttgart, serena.gambarelli@iwb.uni-stuttgart.de

مُسْتَخْلَص

تمت محاكاة الصدأ في وصلات التراكب في الخرسانة المسلحة بإستخدام نموذج كيميائي-رطوبي-حراري-ميكانيكي ثلاثي الأبعاد من العناصر المحددة. تم إستخدام النموذج لفهم الخواص اللاميكانيكية مثل كثافة تيار الصدأ والتمدد الناتج من الصدأ في وصلات التراكب في الخرسانة المسلحة هذا بالإضافة إلي الخواص الميكانيكية المتمثلة في شكل الشقوق الناجمة بفعل صدأ الحديد في الخرسانة وكيفية نشوء تلك الشقوق. كذلك أعطت مقارنة التشققات في النموذج نتائج جيدة عند مقارنتها مع تجارب سابقة.

ABSTRACT

Three-dimensional chemo-hygro-thermo-mechanical finite element model was developed to simulate the accelerated corrosion in lap splice joints in concrete. The model is used to understand non-mechanical properties such as corrosion current intensity and corrosion expansion at the lap splice joint in addition to the mechanical properties such as corrosion cracking and crack propagation at different corrosion levels. Good agreement was found between the model results of the pattern in concrete surface and previous experimental results from the literature.

Keywords: *corrosion, cracks, lap splice, concrete, FE modelling*

1 Introduction

Corrosion of steel bars in reinforced concrete (RC) structures is one of the major causes of concrete premature failures in aggressive environments. It is impaired the durability of the structure and adversely influences their residual strength [1]. Extensive research work has been carried to understand the behaviour of the corrosion of single and multiple bars in concrete, however, corrosion at lap splice joint of reinforcement in concrete received little attention [2]. All of the literature consider corrosion of lap joints in RC beams [3–7] are primarily designed to study the structural capacity of RC elements. It is noted that, the corrosion mechanism at lap joints and consequences in concrete and bond strength are not considered numerically and experimentally. None of the presented literature investigated the associated non-mechanical behaviour. Therefore, this study aims to develop a 3D non-linear finite element (FE) model considering mechanical and non-mechanical behaviour to simulate the corrosion at splice joint along with experimental validation. The model results will help to improve the understanding of the behaviour of corroded splices in RC structures and help to develop effective tools to predict the residual strength of the corroded structures.

2. Modelling of steel corrosion in concrete

2.1 Corrosion Mechanism

Steel in concrete is normally protected from corrosion by a film layer of ferric oxide known as a passive layer [8]. This layer can be broken (i.e. depassivation) by carbonation of concrete cover, or by penetration of chloride through cracks, or by sulphide iron attack, or by stray of direct electrical current [1]. Once the depassivation occurred the corrosion may develop. The location at which the passive layer breaks forms the anode. At this location, the steel atoms release electrons in an anodic reaction with the corrosion medium and become ions as represented in Eq. (1), [9].

$$Fe \rightarrow Fe^{2+} + 2e^{-} \quad (1)$$

The cathode is formed at the intact passive layer, and consumes the two electrons in presence of water and oxygen to form hydroxyl ions (OH^{-}).

$$2e^{-} + H_2O + \tfrac{1}{2} O_2 \rightarrow 2OH^{-}. \quad (2)$$

The hydroxyl ions (OH^{-}) react with the ferrous ions (Fe^{2+}) producing Ferrous Hydroxide, $Fe(OH)_2$, Eq. (3). And then a couple of reactions occur to form Ferric Hydroxide $Fe\ (OH)_3$, Eq. (4), and the Hydrated Ferric Oxide, the red rust, Eq. (5). The process is entirely illustrated in Figure 1.

$$Fe^{2+} + 2OH^{-} \rightarrow Fe(OH)_2 \quad (3)$$

$$4Fe(OH)_2 + O_2 + 2H_2O \rightarrow 4Fe\ (OH)_3 \quad (4)$$

$$4Fe(OH)_3 \rightarrow Fe_2O_3.H_2O + 2H_2O \quad (5)$$

To model the corrosion process (i.e. depassivation, reduction of bar cross-section, and inflation of the corrosion product), the corrosion rate it has to be estimated using the corrosion current density. Considering the mentioned process in Equation (1) to (5) and the illustration in Figure 1, in order to calculate the corrosion current density the following non-mechanical (i.e. physical and electrochemical) and mechanical process should be modelled [8]:

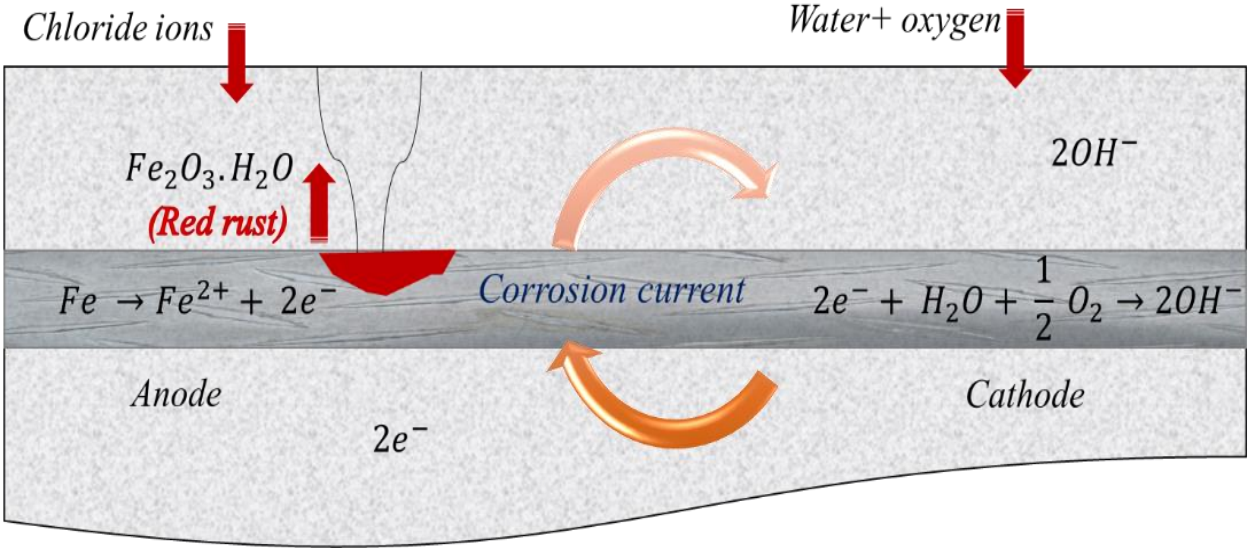

Figure 1: Generalisation of corrosion process

1) Diffusion of oxygen, chloride ions, and pore water through the concrete cover;

2) Diffusion of ferrous hydroxide near steel surface;

3) The depassivation of steel due to critical chloride ion concentration;

4) The cathodic and anodic electric potentials depending on oxygen and ferrous hydroxide concentrations;

5) The polarization of electrodes due to changes in concentration of oxygen and ferrous hydroxide;

6) The flow of electric current through the electrolyte in pores of concrete;

7) The mass sinks or sources of oxygen, ferrous hydroxide, and hydrated red rust near the electrodes, based on Faraday law; and

8) The rust production rate, based on reaction kinetics (concrete cracking).

To model these processes realistically, the chemo-hygro-thermal process have to be coupled with the mechanical consequences (CHTM). The coupling should account for the change of concrete properties due to chemo-hygro-thermal effects in addition to the corrosion induced cracking in concrete.

2.2 CHTM model for corrosion in concrete

In this study, the 3D chemo-hygro-thermo-mechanical FE model developed in [10–12] will be utilised. The model shows realistic simulations of the process before [10] and after depassivation [11] as well as the concrete damage induced by transportation of corrosion products through concrete pores and cracks [12]. The model is also extensively validated considering single bar without [13] and with stirrups [14] and multiple bar arrangement [15] taking into account determination of the critical anodic and cathodic areas [13–16].

The model was implemented into a 3D finite element code. The non-mechanical part of the problem is solved by using direct integration method of implicit type. To solve the mechanical part, Newton-Rapshon iterative scheme is used. As a constitutive law the micro-plane model for concrete is used [17]. To avoid mesh size dependency as a regularization method simple crack band approach is employed. Coupling between mechanical and non-mechanical part of the model is performed by continuous update of governing parameters during the incremental transient finite element analysis using staggered solution scheme (Figure 2). For more detail see [13–15].

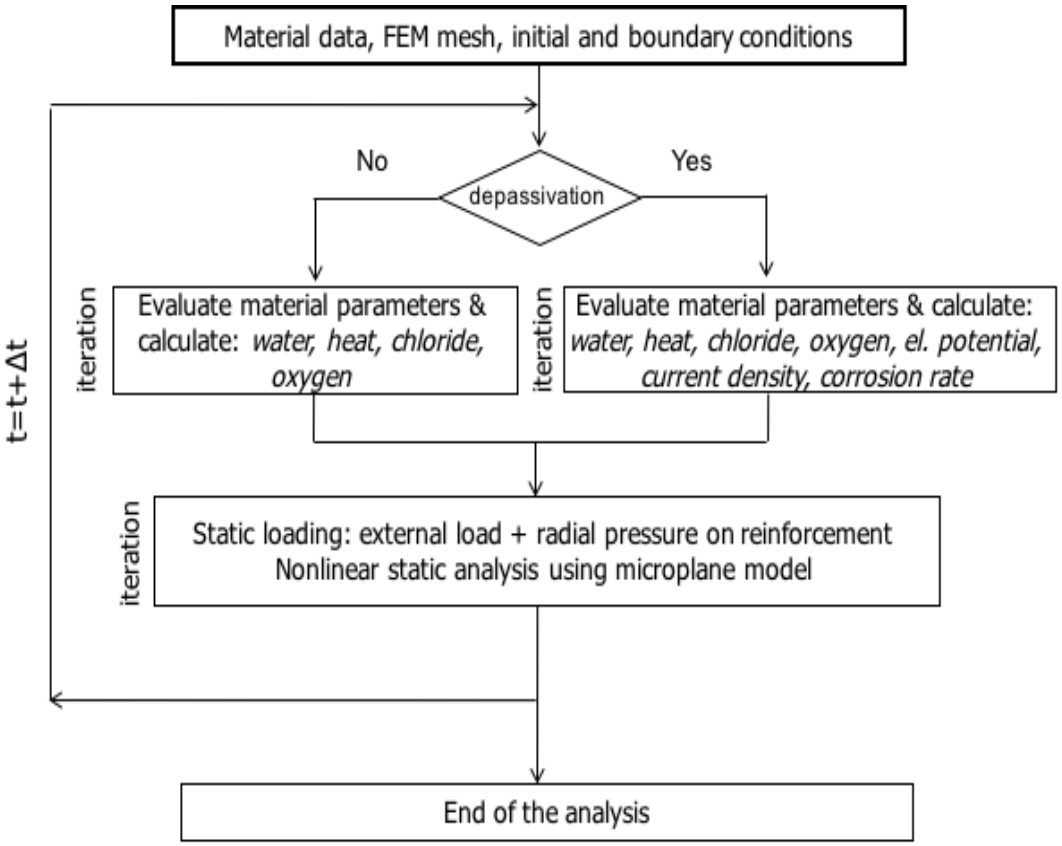

Figure 2: Computational framework of the 3D CHTM FE model

3. CHTM 3D FE model for accelerated corrosion at lap spliced joint

A non-linear 3D CHTM model of a concrete beam was simulated using the non-commercial finite element software package MASA which is developed at the University of Stuttgart (Institute of Construction Materials, IWB).

The simulations used the same beam properties and follow a similar procedure adopted in the experiments in [5], Figure 3. The experiment on 200x300 mm RC beam section with a length of 450 mm and reinforced with 20 mm steel bar and 30 mm concrete cover will only be presented in this paper.

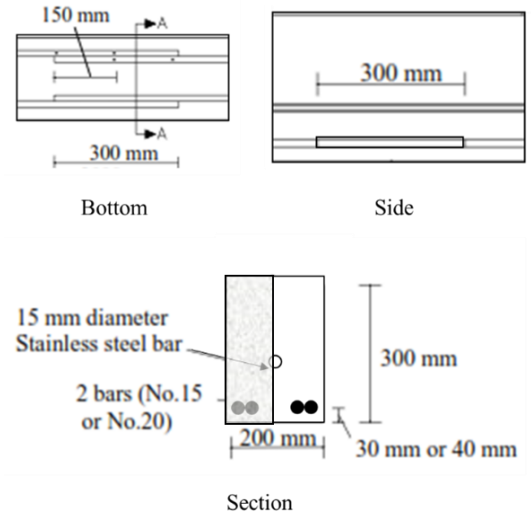

Figure 3: Experiment setup for lapped spliced joint specimen [5]

To reduce the computational cost, the model simulate only half width of the beam. (Figure 3). Because the concrete section is not similar along the length, the concrete is modelled using 4-node tetrahedral solid elements considering the non-linear behaviour. Both steel rebar and stainless steel tube are modelled using 8-node hexagonal solid element with linear properties, as only minor stresses are expected.

The radial expansion of corrosion product is modelled using 1D radially oriented contact element with a length of 0.1 mm [16]. The radial expansion in the contact element Δl_r is calculated using Equation (6), [18]. Where m_r the mass of rust, A_r is the surface area of corroded steel under consideration.

$$\Delta l_r = 4.44 \times 10^{-4} \frac{m_r}{A_r} \quad (6)$$

The mass of rust $m_r\ (kg)$ produced for a rust rate $J_r\ (kg/m^2 s)$ of over a time interval of $\Delta t\ (s)$ could be calculated as [12]:

$$m_r = J_r \Delta t A_r \quad (6)$$

Where J_r is calculated using corrosion current density $i_a\ (A/m^2)$ in the chemical reactions in Equation (3) and (4) and the Faraday's law as:

$$J_r = 5.536 \times 10^{-7} i_a \quad (7)$$

4. Model results and Discussion

The results of the simulation of the corrosion process starting from the non-mechanical properties such as corrosion current density, rust product and mechanical properties in terms of corrosion crack pattern, and corrosion crack propagation at the lap spliced zone are discussed in this section.

4.1 Corrosion current density

The distribution of the current density (A/m^2) in the chemical reactions in Equation (3) and (4) at the splice joint at the middle length is shown in Figure . It is clear that the current distribution in the spliced steel bars (i.e. anode) has been influenced by the location of the stainless steel which is served as a cathode at the top. This forced the corrosion current (i.e. free electrons) to flow between the stainless steel and steel bars from up-right to down left. This could easily be imagined as if there is a spot light illuminated at the cathode. The figure also shows how the intensity of the corrosion current is too high at the surface facing the cathode (i.e. spot light) compare to the surface not facing or hidden behind the right bar (surface at shadow). This directly influence the production of the rust and thereby the development of corrosion cracking.

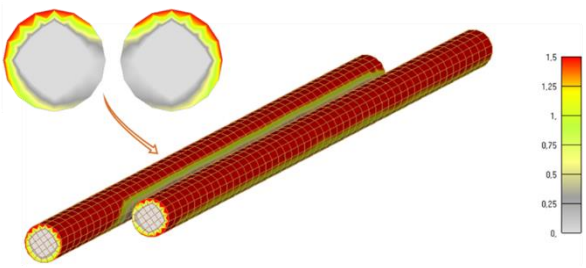

Figure 4: Corrosion current intensity through the length of the lapped splice joint (A/m^2)

4.2Expansion of corrosion product

Figure 5 shows the expansion of rust production at the middle of the splice joint. As expected, the corrosion product was found to follow non-uniform distribution similar to that of current intensity shown in Figure 4. The produced corrosion product usually expands 2-7 times larger than the volume of steel. Therefore, corrosion induced stresses and cracking takes place into the concrete surrounding steel bars and ultimately concrete cracks or spalling may take place.

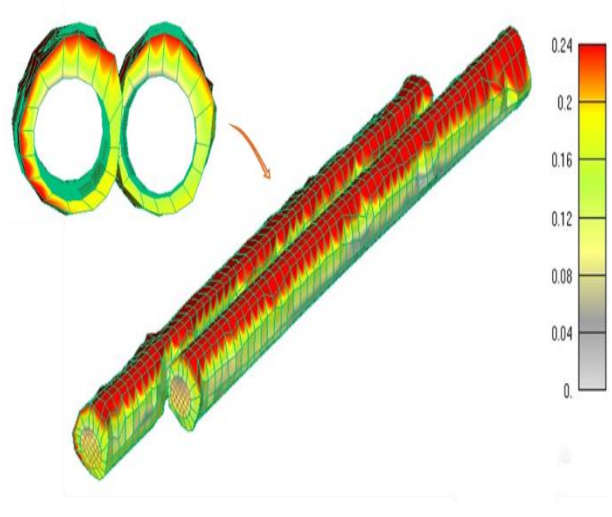

Figure 5: Rust expansion at the lapped splice joint (mm)

4.4 Corrosion crack pattern at concrete surface

The crack pattern in both model results and experiment are compared. Cracks pattern at the bottom of the beam subjected to accelerated corrosion is shown in Figure 6. The predictions of the 3D FE CHTM model is in a good agreement with the experimental results. This pattern could even be understood utilising the model to monitor how corrosion cracks are propagated.

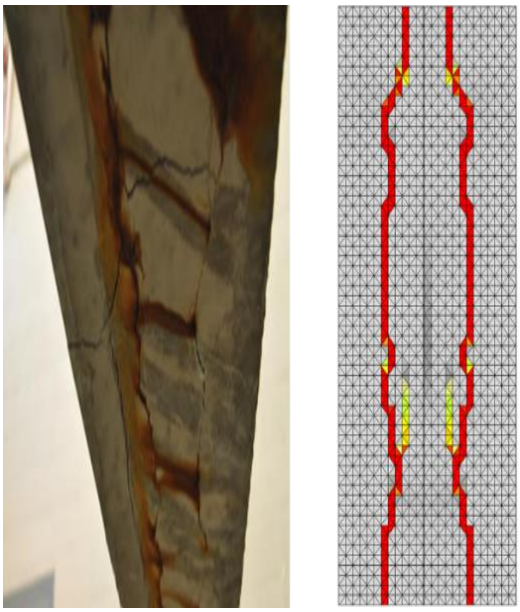

Figure 6: Crack pattern at the bottom face D20-C30 in experiment [5] **(left) and mirrored model (right)**

4.5 crack propagation into surrounding concrete

The crack propagation is monitored in the beam at different corrosion levels (percentages are calculated using Equation 7) as shown in Figure 7. It is clear that internal crack toward the centre start first followed by the bottom crack at 0.85% and continue to widening with potential of side crack at the late stages. The cracks in the last step (i.e. 3.3% corrosion level) was mirrored to visualise the spalling failure mode which is discussed above.

This pattern of the external cracks (Figure 6) and that of internal cracks, Figure 5, along with suggest that the failure mode in this case is likely to be spalling of concrete between splices at the bottom face or at the corner. This could be clearly represented by plotting the deformed shape at the splice zone, Figure 8. Also, Figure 8 shows the locations where the rust build up its product

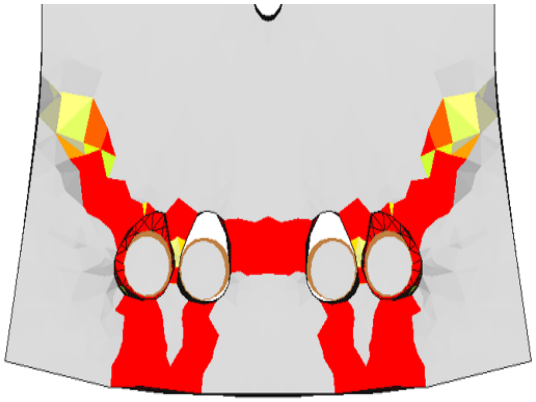

Figure 8: Deformed shape at the middle of splice joint showing corrosion cracks

5 Conclusion

The accelerated corrosion at lapped splice joint is simulated using a coupled 3D chemo-hygro-thermo-mechanical (CHTM) finite element (FE) model and the results are compared to previous experimental data from the literature. The comparison shows that the model is able to realistically replicate the corrosion induced cracking in concrete. The model was used to understand the mechanism of corrosion in terms of distribution of the current density, rust product, and rust expansion in the splice zone and where rust is accumulated. The model was then used to understand the crack propagation at different corrosion levels at the joint. It is found that the corrosion at the lap splice joint is influenced by the location of the cathode where the chloride ions ingress to the joint.

Acknowledgment

Authors gratefully acknowledge the support of TWAS-DFG collaboration visit program for supporting this work.

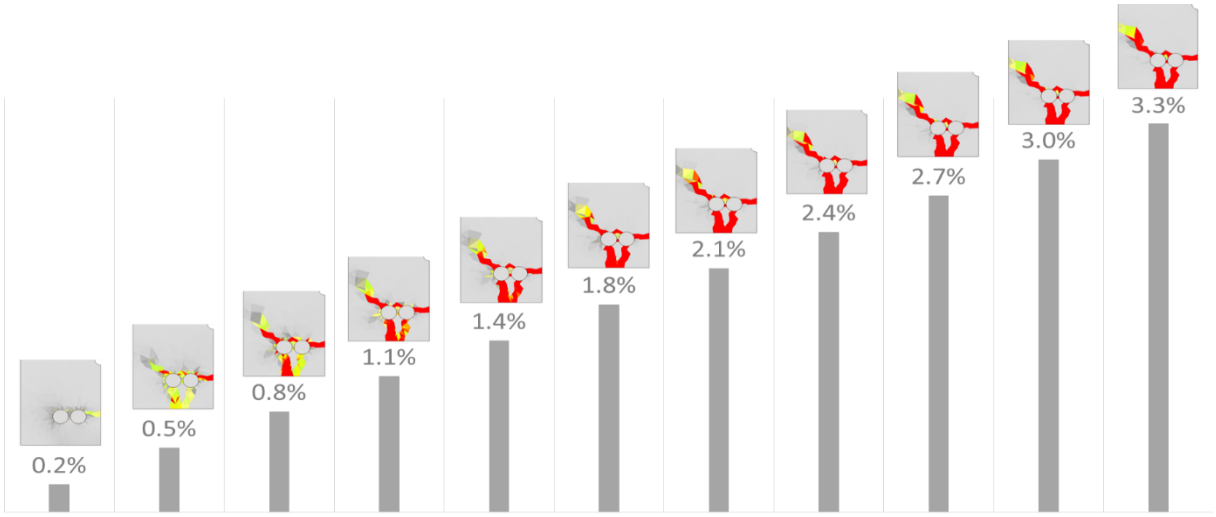

Figure 7: Cracks propagation at different corrosion levels for Beam D20-C30

References

[1] FIP, Bond of reinforcement in concrete - State of art report, International Federation For Structural Concrete, 2000.

[2] S. Sajedi, Q. Huang, Load-Deflection Behavior Prediction of Intact and Corroded RC Bridge Beams with or without Lap Splices Considering Bond Stress-Slip Effect, J. Bridg. Eng. 22 (2017). doi:10.1061/(ASCE)BE.1943-5592.0000981.

[3] A. Kawamura, K. Maruyama, S. Yoshida, T. Masuda, Residual capacity of concrete beams damaged by salt attack, Concr. under Sev. Cond. (1995) 1448–1457.

[4] J. Rodriguez, L. Ortega, J. Casal, Load carrying capacity of concrete structures with corroded reinforcement, Constr. Build. Mater. 11 (1997) 239–248. doi:10.1016/S0950-0618(97)00043-3.

[5] A. Shihata, CFRP strengthening of RC beams with corroded lap spliced steel bars, UWSpace, 2011.

[6] T. Shimomura, Y. Tanaka, T. Yamaguchi, Residual structural performance of deteriorated RC bridge girder with reinforcement corrosion, in: P.M. M.G. Alexander, H.-D. Beushausen, F. Dehn (Ed.), Concr. Repair, Rehabil. Retrofit. III, Taylor & Francis Group, 2014: pp. 295–296.

[7] Y. Tanaka, T. Shimomura, T. Yamaguchi, Loading Test of RC Beam Bridge Built 80 Years Ago in Japanese Coastal Area, in: C. Andrade, G. Mancini (Eds.), Model. Corroding Concr. Struct. Proc. Jt. Fib-RILEM Work. Held Madrid, Spain, 22--23 Novemb. 2010, Springer Netherlands, Dordrecht, 2011: pp. 159–177. doi:10.1007/978-94-007-0677-4_11.

[8] Z. Bazant, Physical model for steel corrosion in concrete sea structures - Theory, J. Struct. Div. (1979).

[9] J.P. Broomfield, Corrosion of steel in concrete: understanding, investigation, and repair, 2nd Editio, E & FN Spon, New York, 2007.

[10] J. Ožbolt, G. Balabanić, G. Periškić, M. Kušter, Modelling the effect of damage on transport processes in concrete, Constr. Build. (2010).

[11] J. Ožbolt, G. Balabanić, M. Kušter, 3D Numerical modelling of steel corrosion in concrete structures, Corros. Sci. (2011).

[12] J. Ožbolt, F. Oršanić, G. Balabanić, M. Kušter, Modeling damage in concrete caused by corrosion of reinforcement: coupled 3D FE model, Int. J. (2012).

[13] J. Ožbolt, F. Oršanić, G. Balabanić, Modeling pull-out resistance of corroded reinforcement in concrete: Coupled three-dimensional finite element model, Cem. Concr. Compos. (2014).

[14] J. Ožbolt, F. Oršanić, G. Balabanić, Modelling processes related to corrosion of reinforcement in concrete: coupled 3D finite element model, Struct. Infrastruct. (2016).

[15] J. Ožbolt, F. Oršanić, G. Balabanić, Modeling corrosion-induced damage of reinforced concrete elements with multiple-arranged reinforcement bars, Mater. Corros. (2016).

[16] J. Ožbolt, G. Balabanić, E. Sola, Determination of critical anodic and cathodic areas in corrosion processes of steel reinforcement in concrete, Mater. Corros. (2016).

[17] J. Ožbolt, Y. Li, I. Kožar, Microplane model for concrete with relaxed kinematic constraint, Int. J. Solids Struct. 38 (2001) 2683–2711. doi:https://doi.org/10.1016/S0020-7683(00)00177-3.

[18] A.O. Abdelatif, J. Ožbolt, S. Gambarelli, 3D finite element modelling of corrosion of lap splice joints in concrete, Constr. Build. Mater. 169 (2018). doi:10.1016/j.conbuildmat.2018.02.150.